

AD-A255 179



2

AEROSPACE REPORT NO.
TR-0091(6940-06)-2

SEP 1 8 1992

The Relationship Between Electrostatic Discharges on Spacecraft P78-2 and the Electron Environment

Prepared by

H. C. KOONS and D. J. GORNEY

Space and Environment Technology Center
Technology Operations

15 March 1992

Prepared for

SPACE AND MISSILE SYSTEMS CENTER
(formerly Space Systems Division)
AIR FORCE MATERIEL COMMAND
Los Angeles Air Force Base
P. O. Box 92960
Los Angeles, CA 90009-2960

Engineering and Technology Group

THE AEROSPACE CORPORATION
El Segundo, California

APPROVED FOR PUBLIC RELEASE;
DISTRIBUTION UNLIMITED

92-25243




2 9 15 021

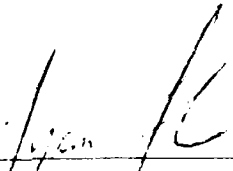
This report was submitted by The Aerospace Corporation, El Segundo, CA 90245-4691, under Contract No. F04701-88-C-0089 with the Space Systems Division, P. O. Box 92960, Los Angeles, CA 90009-2960. It was reviewed and approved for The Aerospace Corporation by A. B. Christensen, Principal Director, Space and Environment Technology Center. Capt. T. Fisher was the project officer for the Mission-Oriented Investigation and Experimentation (MOIE) program

This report has been reviewed by the Public Affairs Office (PAS) and is releasable to the National Technical Information Service (NTIS). At NTIS, it will be available to the general public, including foreign nationals.

This technical report has been reviewed and is approved for publication. Publication of this report does not constitute Air Force approval of the report's findings or conclusions. It is published only for the exchange and stimulation of ideas.



QUANG BUI, Lt, USAF
MOIE Program Manager



TYRON FISHER, CAPT, USAF
MOIE PROJECT OFFICER

UNCLASSIFIED

SECURITY CLASSIFICATION OF THIS PAGE

REPORT DOCUMENTATION PAGE

1a. REPORT SECURITY CLASSIFICATION Unclassified			1b. RESTRICTIVE MARKINGS		
2a. SECURITY CLASSIFICATION AUTHORITY			3. DISTRIBUTION/AVAILABILITY OF REPORT Approved for public release; distribution unlimited		
2b. DECLASSIFICATION/DOWNGRADING SCHEDULE					
4. PERFORMING ORGANIZATION REPORT NUMBER(S) TR-0091(6940-06)-2			5. MONITORING ORGANIZATION REPORT NUMBER(S) SMC-TR-92-35		
6a. NAME OF PERFORMING ORGANIZATION The Aerospace Corporation Technology Operations		6b. OFFICE SYMBOL <i>(If applicable)</i>	7a. NAME OF MONITORING ORGANIZATION Space and Missile Systems Center		
6c. ADDRESS (City, State, and ZIP Code) El Segundo, CA 90245-4691			7b. ADDRESS (City, State, and ZIP Code) Los Angeles Air Force Base Los Angeles, CA 90009-2960		
8a. NAME OF FUNDING/SPONSORING ORGANIZATION		8b. OFFICE SYMBOL <i>(If applicable)</i>	9. PROCUREMENT INSTRUMENT IDENTIFICATION NUMBER F04701-88-C-0089		
8c. ADDRESS (City, State, and ZIP Code)			10. SOURCE OF FUNDING NUMBERS		
			PROGRAM ELEMENT NO.	PROJECT NO.	TASK NO.
			WORK UNIT ACCESSION NO.		
11. TITLE (Include Security Classification) The Relationship Between Electrostatic Discharges on Spacecraft P78-2 and the Electron Environment					
12. PERSONAL AUTHOR(S) Koons, Harry C. and Gorney, David J.					
13a. TYPE OF REPORT		13b. TIME COVERED FROM _____ TO _____		14. DATE OF REPORT (Year, Month, Day) 92 March 15	
				15. PAGE COUNT 24	
16. SUPPLEMENTARY NOTATION					
17. COSATI CODES			18. SUBJECT TERMS (Continue on reverse if necessary and identify by block number)		
FIELD	GROUP	SUB-GROUP			
			Spacecraft charging, Electrostatic discharges, Neural network, Geosynchronous orbit		
19. ABSTRACT (Continue on reverse if necessary and identify by block number) The relationship between the energetic electron environment and electrostatic discharges on the P78-2 (SCATHA) spacecraft has been examined. Internal discharges occur near perigee while surface discharges occur about uniformly over the radial range covered by SCATHA, 5.5 to 8 Re. The surface discharges peak at local midnight and decrease toward local morning while the internal discharges have a broad occurrence maximum centered on local noon. Both types are far more likely to occur when the Earth's magnetic field is disturbed. Although few surface discharges occur when the Planetary Magnetic Index, Kp, is less than 4, a modest number of internal discharges occur under these quiet to normal conditions. In all cases where internal discharges occurred under quiet to normal conditions, a period of very disturbed conditions had occurred a few days earlier. Surface discharges have a strong tendency to occur when the flux of electrons with energies of 10's of keV is high while internal discharges occur when the flux of electrons with energies of 100's of keV is high, and the flux of 10's of keV electrons is low. A significant correlation has been found between the occurrence of discharges on SCATHA and an estimate of the energetic electron fluence at geosynchronous					
20. DISTRIBUTION/AVAILABILITY OF ABSTRACT <input checked="" type="checkbox"/> UNCLASSIFIED/UNLIMITED <input type="checkbox"/> SAME AS RPT. <input type="checkbox"/> DTIC USERS				21. ABSTRACT SECURITY CLASSIFICATION Unclassified	
22a. NAME OF RESPONSIBLE INDIVIDUAL		22b. TELEPHONE (Include Area Code)		22c. OFFICE SYMBOL	

UNCLASSIFIED

UNCLASSIFIED

SECURITY CLASSIFICATION OF THIS PAGE

orbit obtained from a neural network model of the relativistic electron flux at geosynchronous orbit. At predicted daily fluences greater than 1010 elec/cm² almost all discharges result from internal charging. The incidence of internal discharges at predicted daily fluences above 1010 elec/cm² is sufficiently high to warrant the use of this predictor to issue warnings for real time satellite operations. The statistics of nine years of surface discharges on the SCATHA spacecraft are dominated by the single charging event on September 22, 1982. The largest amplitude discharges and the most serious satellite anomalies occurred during this event while the spacecraft was in sunlight near perigee at 0400 local time.

UNCLASSIFIED

SECURITY CLASSIFICATION OF THIS PAGE

PREFACE

The authors thank P. Mizera of the Aerospace Corporation for the data from the SSPMs and J. B. Reagan, R. Sharp and R. Nightingale of Lockheed for the data from the High Energy Particle Spectrometer and the Energetic Ion Composition Experiment. We also thank R. Klebesadel, D. Baker, and J. B. Blake for the electron data from spacecraft 1982-019 that was used to generate the neural network model. We wish to thank M. Schulz for useful discussions on relativistic electron intensities in the outer radiation belt. The values of Kp used in this study were obtained from NOAA's Environmental Data and Information Service, National Geophysical Data Center. This work was supported by the Space Systems Division of the U. S. Air Force under Contract No. F04701-88-C-0089.

THIS QUALITY INSPECTED

CONTENTS

PREFACE.....	1
INTRODUCTION.....	5
DATA.....	7
NATURAL CHARGING.....	9
ELECTRON DATA.....	13
HIGH ENERGY ELECTRON ESTIMATOR.....	17
SUMMARY.....	21
REFERENCES.....	23

FIGURES

1. Amplitude distribution of pulses due to surface and internal discharges.....	10
2. Radial distribution of (a) surface and (b) internal discharges.....	10
3. Local time distribution of (a) surface and (b) internal discharges.....	11
4. Kp distribution of (a) surface and (b) internal discharges.....	12
5. Distribution of (a) surface and (b) internal discharges as a function of the count rate of 18.4 keV electrons	13
6. Distribution of (a) surface and (b) internal discharges as a function of the flux of 288 keV electrons	14
7. Scatter plot of discharges as a function of the 18.4 keV and 288 keV count rates. The solid squares are overlapping hollow squares and solid circles.....	14
8. Occurrence of discharges as a function of the daily fluence of electrons with energies greater than 300 keV as estimated by a linear prediction filter model.....	18
9. Occurrence of discharges as a function of the daily fluence of electrons with energies greater than 300 keV as estimated by neural network model	19

TABLE

1. Distribution of Pulses Detected by the Pulse Analyzer in 1,527 Days of Analyzed Data.....	7
---	---

INTRODUCTION

Electrons in the space environment charge materials on the surface and inside a spacecraft. When the resulting electric field exceeds the breakdown field intensity for the material, an electrostatic discharge occurs. Electrostatic discharges are believed to have been responsible for a large number of spacecraft anomalies, including command errors, phantom commands, degraded sensor performance, parts failure, and even complete loss of mission on a variety of spacecraft.^{1,2,3}

DeForest⁴ was the first to observe surface charging on a geosynchronous satellite. He found that ATS-5 charged to potentials as high as 10,000 V in eclipse, and as high as 200 V in sunlight. He also noted that insulators near the aperture of his electron detector could be charged to several hundred volts without an accompanying change in the over-all spacecraft potential. The first discharges aboard a satellite were reported by Shaw et al.⁵ They detected discharges that occurred in the vicinity of transient sensors. The number of discharges increased during geomagnetically disturbed times and correlated with the anomalous behavior of subsystems on the spacecraft. Garrett⁶ has reviewed the theory and measurements of the charging of spacecraft surfaces.

Vampola⁷ showed that the occurrence of anomalies onboard the U. S. Air Force Defense Support Program satellites coincided with significant increases in the flux of electrons greater than 1.2 MeV as measured by the GOES spacecraft and concluded that the anomalies were caused by thick dielectric charging. Thick dielectric charging, or internal charging as we refer to it in this report, occurs when energetic electrons embed within dielectrics. This can build up electric fields inside a dielectric until its breakdown field intensity is reached.⁸ Penetrating electrons can also charge well-insulated floating conductors below the surface of the vehicle.⁹ Electromagnetic interference from the resulting electrostatic discharges is responsible for the anomalies.

In order to improve our understanding of the relationship between the environment and electrostatic discharges, we have examined the data from the P78-2 (SCATHA -- Spacecraft Charging at High Altitudes) Pulse Analyzer, Satellite Surface Potential Monitors, the Energetic Ion Composition Experiment, and the High Energy Particle Spectrometer for a relationship between discharges and the electron environment. The SCATHA satellite was launched on Jan. 30, 1979. The primary objective of the mission was to obtain environmental and engineering data that could be used for design guidelines and specifications to ensure that future spacecraft will operate satisfactorily in the plasma environment at synchronous orbit. The experiments are described by Stevens and Vampola¹⁰ and Fennell.¹¹

The engineering payloads include a Pulse Analyzer that measures the characteristics of electrical pulses in both the frequency and time domains. It measures the number of pulses, their amplitudes, and their shapes with four sensors. It has been operating continuously since Feb. 1979. Since that time, data from 1527 days have been analyzed. Pulses have been detected in response to spacecraft commands, during electron and ion beam operations, and during periods of natural surface charging. Previous publications have documented the occurrence of pulses during the first two years of operation of the vehicle, their amplitudes, pulse shapes, and the correlation of these pulses with time periods when the surface samples on the vehicle are charged.^{12,13,14}

The Satellite Surface Potential Monitors (SSPMs) measure the voltage between the surface of selected materials, such as Kapton, Teflon, and quartz fabric, and the ground frame of the spacecraft. The spacecraft contains three SSPMs, two on the cylindrical side of the vehicle and one on top. Those on the side of the vehicle move into and out of sunlight as the vehicle rotates at one rpm. The one on top was essentially always shadowed by the vehicle. All three contain Kapton samples and the one on top also contains a quartz fabric sample. The Kapton and the quartz fabric samples are used in the study reported here to determine if the surface of the vehicle is charged.

The Energetic Ion Composition Experiment measures 100 eV to 32 keV ions. The instrument also includes four broadband electron channels from 0.07 to 24 keV.^{10,11} The High Energy Particle Spectrometer has four solid-state detectors to measure the energetic electron and proton distributions. The various particles and energy ranges are measured in command-selectable, time-multiplexed modes. The instrument covers electron energies from 0.05 to 10 MeV and protons from 1 to 200 MeV.^{10,11}

DATA

Pulse Analyzer data from a total of 1527 days between Feb. 1979 and Mar. 1988 have been analyzed. Data were collected continuously for most of that time period. The data analyzed to date represent about 45% of the available data. Essentially the entire first year of data has been analyzed. Following the first year, only selected periods have been analyzed. This selection has included time periods of known anomalies on other synchronous satellites and time periods containing geomagnetically disturbed days. This selection process may bias the statistics of discharge occurrence presented below.

Table 1 contains a summary of the pulses detected by the Pulse Analyzer during those 1527 days. Pulses occurring within one second of a spacecraft command are attributed to a vehicle or payload response to the command and are identified as a command pulse in Table 1. Pulses have also been detected shortly after the time that the ground station command transmitter ceased sending special signals, called s-tones, to the vehicle. These signals enable the space vehicle command receiver. Those pulses are identified as s-tones in Table 1. The majority of the remaining pulses listed in Table 1 occurred during operations of the Electron or Ion Beam Experiments.¹⁵ Only 316 of the 8389 pulses cannot be associated with normal vehicle commands or ion and electron beam operations.

Table 1. Distribution of Pulses Detected by the Pulse Analyzer in 1,527 Days of Analyzed Data.

Type	Number
Command Related	3158
s-Tone cessation	2550
Beam Experiments	2365
Natural Discharges	316
Total	8389

NATURAL CHARGING

Many of the pulses that cannot be associated with normal vehicle commands or ion and electron beam operations occurred during periods of natural surface charging, that is, during periods when large potentials between surface samples and the vehicle reference frame were measured by the SSPM. The coincidence of these pulses with time periods when the samples were differentially charged, and the absence of vehicle commands or mode changes at the time of these pulses has led us to conclude with high confidence that most of the pulses are due to electrostatic discharges.¹² Similar pulses have also been detected during electron and ion beam operations when the surfaces of the samples are artificially charged.¹³ Data from the Kapton and the quartz fabric samples on the SSPMs were used to determine if the surface of the vehicle was charged at the time each of the "natural" discharges was detected. If the potential between any of these four samples and the vehicle frame exceeded 100 V, we consider the surface to have been charged. Natural discharges detected when the surface was charged are defined to be surface discharges. Discharges detected when the surface was not charged are defined to be internal discharges. Although the 100 V discrimination level is somewhat arbitrary, the separation into the two classes is generally unambiguous. For almost all instances when the samples were not charged, the potentials of these samples were much less than 100 V and relatively constant. When the samples were charged, the potentials were much greater than 100 V on at least one of the samples and varied over time periods on the order of a minute.

SSPM data were not available for 45 (14%) of the 316 pulses identified as real discharges. Because all of the pulses that occurred when the vehicle was charged are identified as surface discharges, the number of surface discharges has possibly been somewhat overestimated.

The amplitude distribution of the pulses from the natural discharges is shown in Figure 1. The voltage plotted along the x axis is the highest discriminator level exceeded by each pulse. The discriminator levels are spaced by about a factor of 2 in voltage. Generally we find that the amplitudes of the pulses from the surface discharges are larger than the amplitudes of those from the internal discharges at the Pulse Analyzer sensors. The pulses arising from surface discharges were also significantly larger than pulses detected from normal operations of the vehicle.

During a one-hour period on Sept. 22, 1982, 28 pulses were detected while the surface samples on the SSPMs were highly charged. At that time, the planetary magnetic index, K_p , was 8, and the vehicle was located at a radial distance of $5.8 R_e$ between 0400 and 0500 local time. Because these pulses seriously bias the occurrence statistics, they have been removed from the data reported in this paper. The pulses and vehicle anomalies that occurred on SCATHA on Sept. 22, 1982 have been described by Koons et al.¹⁶

The occurrence of discharges as a function of the radial distance of the spacecraft from the center of the Earth is shown in Figure 2. Since the SCATHA satellite has a low inclination (7.5°), the radial distance in Figure 2 is essentially measured in the Earth's equatorial plane. For reference, geosynchronous orbit is at a radial distance of $6.6 R_e$. Surface discharges are relatively evenly distributed over the region of space covered by the SCATHA satellite, 5.2 to 7.8 Earth radii. The

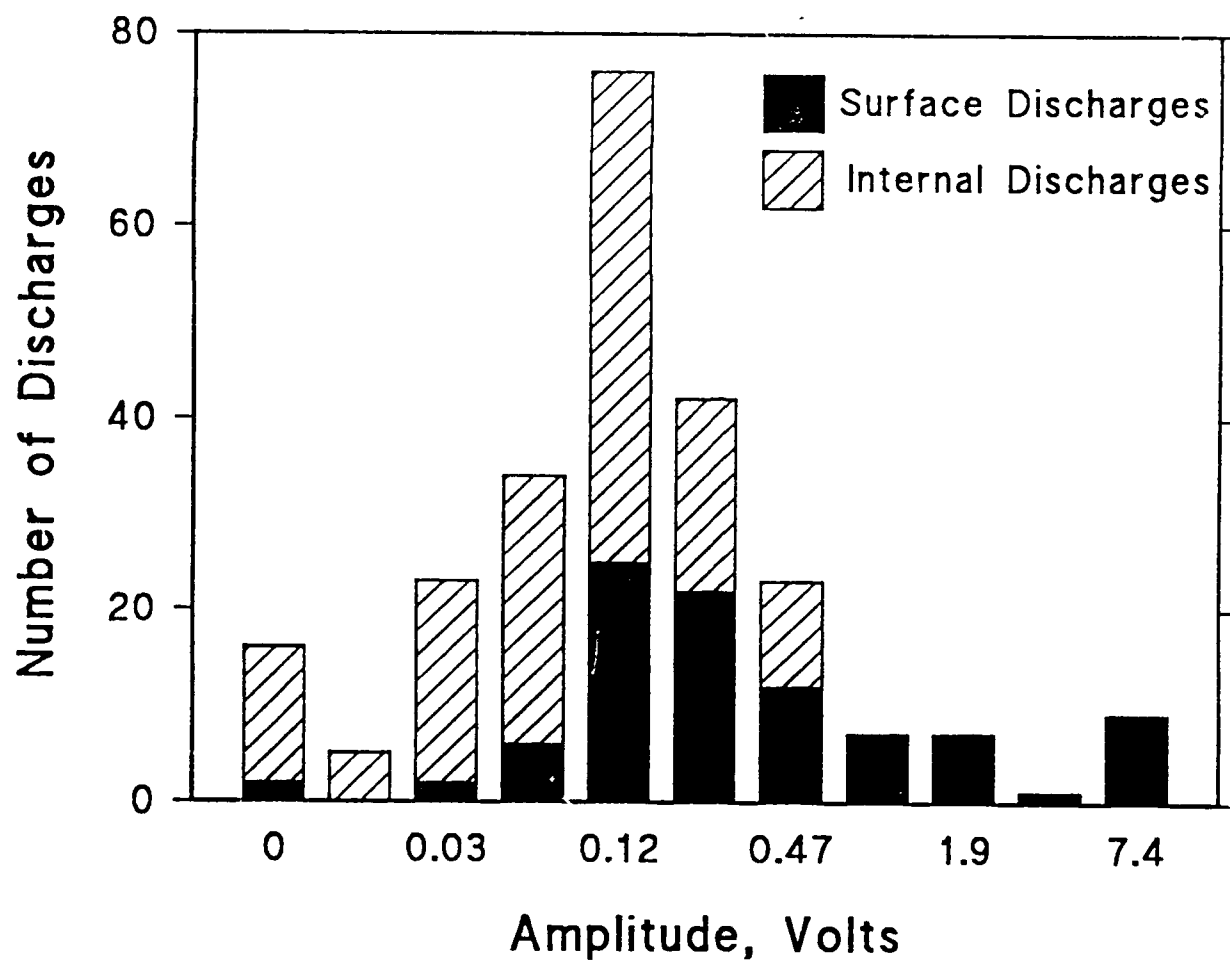


Figure 1. Amplitude distribution of pulses due to surface and internal discharges.

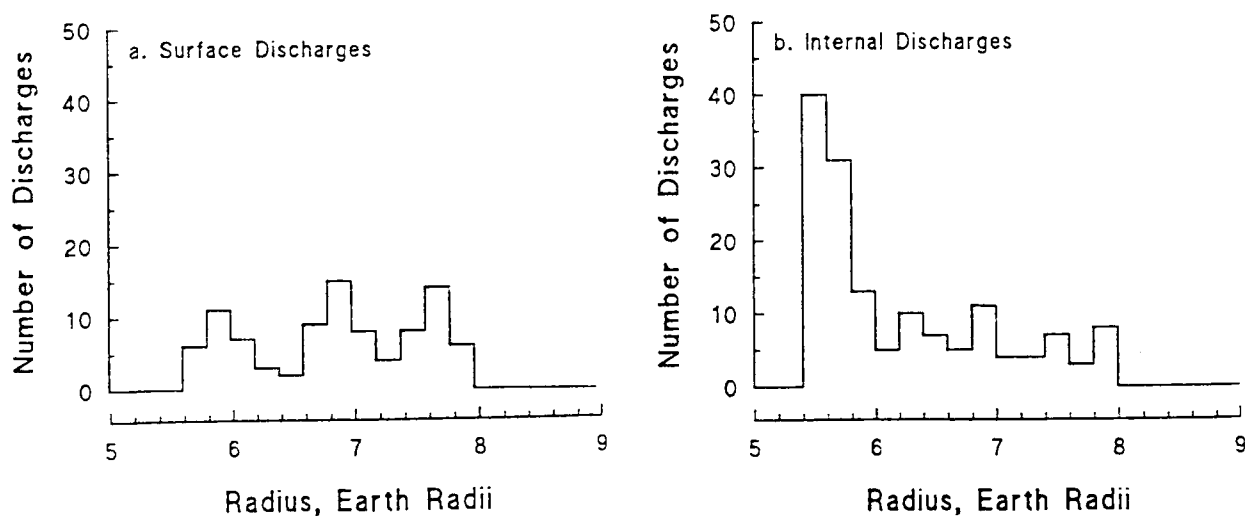


Figure 2. Radial distribution of (a) surface and (b) internal discharges.

number of internal discharges increases dramatically at smaller radial distances, with the largest number occurring near the perigee of the SCATHA satellite. The number of internal discharges increases rapidly toward lower altitudes because the maximum intensity of the outer radiation belt is between $L = 4$ and $L = 5$, i.e., below the perigee of SCATHA. Thus, the vehicle encounters the more energetic electrons of the outer radiation belt as it approaches perigee.

The occurrence of discharges as a function of the local time at the spacecraft is shown in Figure 3. Surface discharges peak strongly at midnight and occur in diminishing numbers into the early morning hours because the electrons responsible for surface charging are injected near geosynchronous orbit near local midnight during a magnetospheric substorm and drift around the morning side of the Earth. Many of the surface discharges at local midnight occurred during the spring and the fall when the spacecraft is eclipsed by the Earth when it is near midnight. Very few surface discharges occurred on the day side of the Earth.

The internal discharges detected on SCATHA occurred preferentially on the day side of the Earth. The maximum in the local-time distribution of internal discharges occurs near noon and thus matches the local-time distribution¹⁷ of relativistic-electron intensities at geosynchronous orbit. At SCATHA's orbit, this asymmetry in local time arises from distortions to the Earth's magnetic field caused by currents on the magnetopause and in the neutral sheet.¹⁸ Because equatorially mirroring electrons drift around the Earth on trajectories of constant B , the day-night asymmetry in the Earth's magnetic field leads to a day-night asymmetry in the geocentric distance to the peak of the outer radiation belt. The peak is at a larger radial distance on the day side than it is at night. Since the spacecraft penetrates further into the outer radiation belt during the day than it does at night, it experiences higher fluxes of relativistic electrons by day than by night. The flux of 0.5 to 1 MeV electrons varies by about an order of magnitude from noon to midnight under magnetically quiet conditions.¹⁹

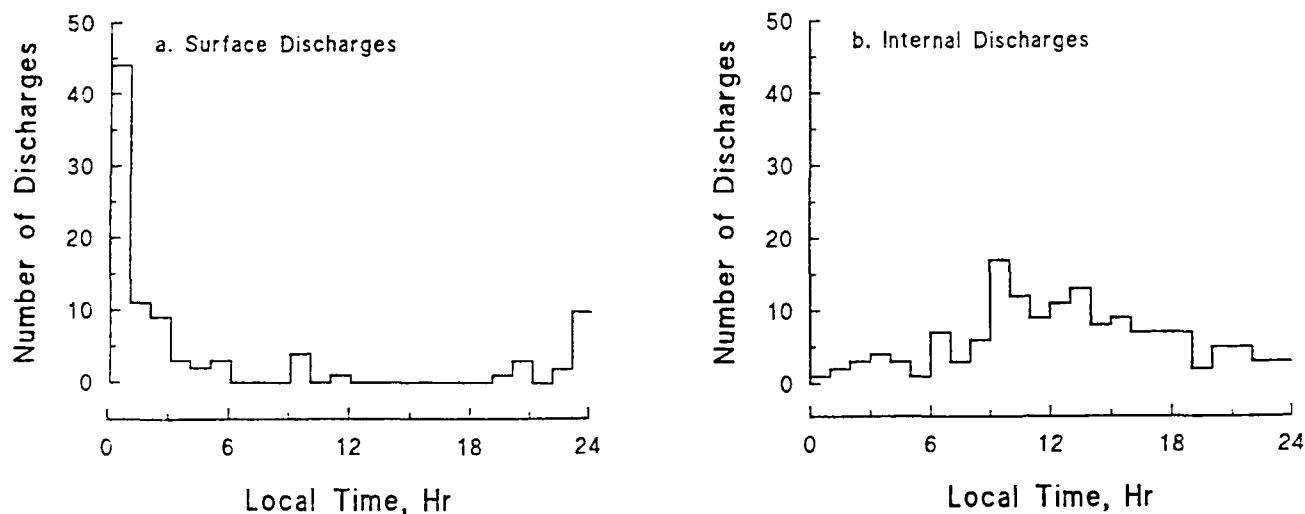


Figure 3. Local time distribution of (a) surface and (b) internal discharges.

Discharges are far more likely to occur when the magnetosphere is active, i.e. when the Planetary Magnetic Index, K_p , is 4 or greater. The solid curves in Figure 4 show the actual number of discharges detected in each category. The dashed curves show the distribution that would have occurred if the discharges were distributed with the same statistical frequency as K_p . The distribution of K_p for the time period from 1932 through 1986 was used to determine the dashed curves in Figure 4. A comparison of the histograms shows that both surface and internal discharges are far more likely to occur when the magnetosphere is active, i.e., when K_p is greater than 4. Very few surface discharges occur below $K_p = 4$. Those that do were most likely caused by electrons injected by small, local sun storms that did not influence the planetary magnetic index, K_p .

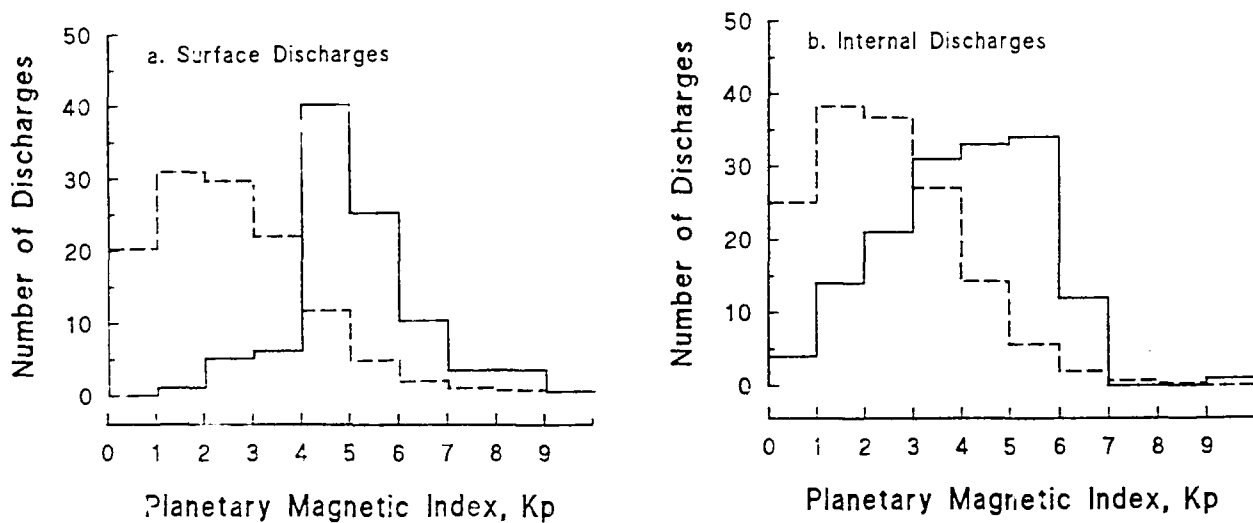


Figure 4. K_p distribution of (a) surface and (b) internal discharges.

ELECTRON DATA

The High Energy Particle Spectrometer^{10,11} on SCATHA measures low-energy (LE) electrons from 50 to 100 keV, medium-energy (ME) electrons from 100 keV to 1 MeV, and high-energy (HE) electrons from 1 MeV to 10 MeV. The Energetic Ion Composition Experiment^{10,11} measures LE electrons from 0.07 to 24 keV. The summary plots of the data from the Satellite Surface Potential Monitor that have been produced over the past decade for the time of each discharge on the spacecraft contain time-series graphs of the count rates for electrons from the 0.18, 0.84, 3.9, 18.4, 57, 140, and 288 keV channels from the Energetic Ion Composition Experiment and the High Energy Particle Spectrometer. The 18.4 keV and the 288 keV channels will be used here to show the relationship between LE and ME electrons and discharges due to surface and internal charging.

Figure 5 shows the number of discharges detected as a function of the count rate of the 18.4 keV electron channel. The number of surface discharges increases dramatically as the flux of 18.4 keV electrons increases. Surface discharges occur above 100 counts per second and dominate the internal discharges for count rates above 1000 counts per second. Bulk discharges occur at low count rates near the threshold of this channel at 10 counts per second and disappear above a count rate of 1000 per second. The flux of ME and HE electrons decreases during the main phase of a geomagnetic storm while the flux of LE electrons increases due to substorm injections of electrons into the inner plasma sheet.^{20,21} This is responsible for the decrease in the number of internal discharges at times when the flux of LE electrons is high. The flux of HE electrons then increases as geomagnetic activity returns to quiet levels following the main phase of a magnetic storm.

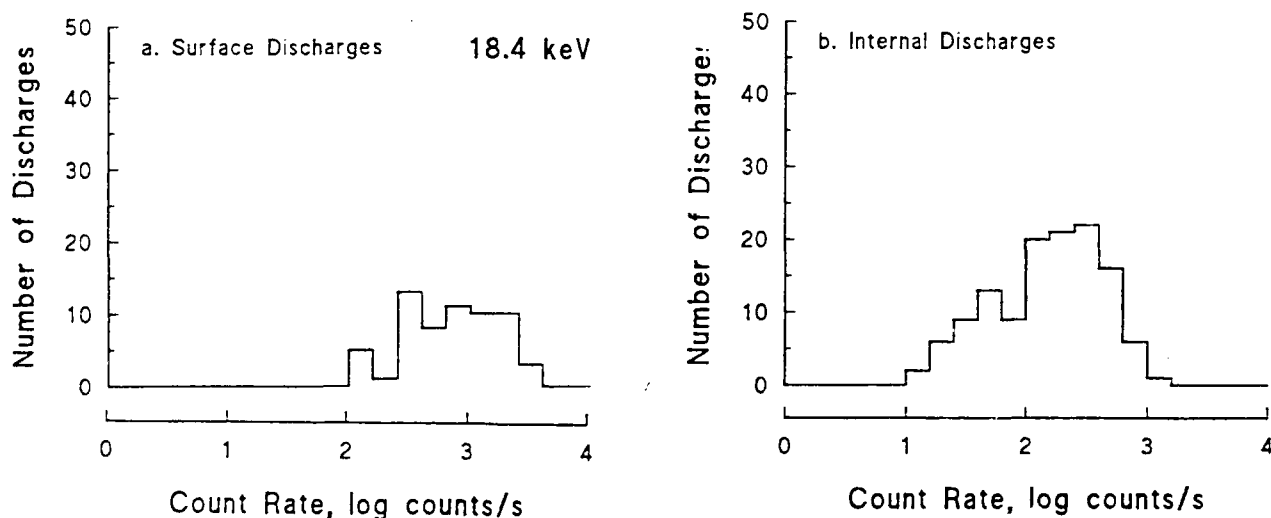


Figure 5. Distribution of (a) surface and (b) internal discharges as a function of the count rate of 18.4 keV electrons.

Figure 6 shows the number of discharges detected as a function of the flux of 288 keV electrons. The number of internal discharges increases dramatically for fluxes above 3600 electrons/(cm²-s-sr-keV), while the number of surface discharges appears for the most part to be unrelated to the flux of 288 keV electrons. Unfortunately, we do not have data from these instruments when discharges were not detected, so it is not possible to convert the data in Figures 5 and 6 to probability distributions.

Figure 7 shows a scatter plot of the discharges with the count rate for the 288 keV electrons on the ordinate and the count rate for the 18.4 keV electrons on the abscissa. All of the surface

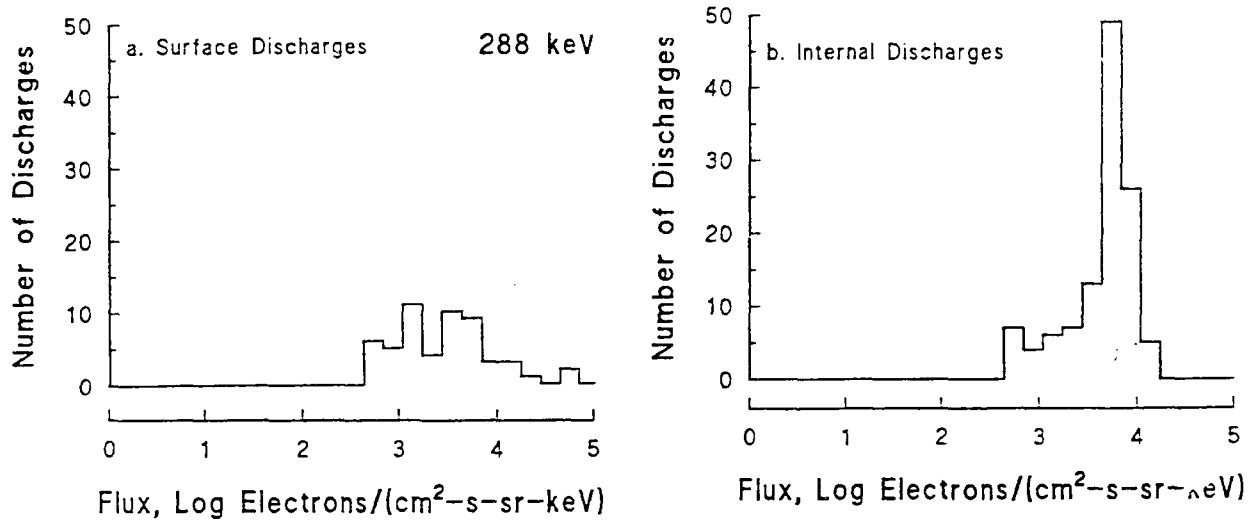


Figure 6. Distribution of (a) surface and (b) internal discharges as a function of the flux of 288 keV electrons.

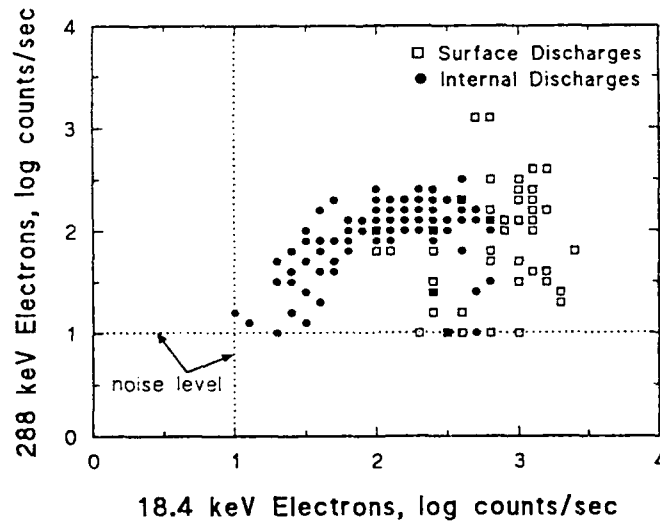


Figure 7. Scatter plot of discharges as a function of the 18.4 keV and 288 keV count rates. The solid squares are overlapping hollow squares and solid circles.

discharges, identified by squares in Figure 7, occur above an 18.4 keV count rate of 100. Once the count rate exceeds 100, there is little correlation between the count rates for the two energies when surface discharges occur. Most of the internal discharges, identified by a solid circle in Figure 7, appear in a relatively limited area of the diagram that increases more slowly in the 288 keV count rate than in the 18.4 keV count rate.

HIGH ENERGY ELECTRON ESTIMATOR

It would be useful to spacecraft operators to be able to forecast days on which internal discharges are likely to occur on spacecraft in synchronous orbit. Internal charging of dielectrics is caused by the build-up of charge within the material. It is related to the fluence of ME and HE electrons over a period comparable to the decay time of the charge in the dielectric. The decay time depends on the resistivity of the material. This may be very large for a material such as Teflon. Thus, internal discharges are expected to be related to the fluence of ME and HE electrons over a period of hours or even days. We have used two techniques, a linear prediction filter and a neural network model, to estimate the daily fluence of ME and HE electrons on days when SCATHA experienced discharges.

Nagai²¹ and Baker et al.²² have used linear prediction filter analysis to predict the relationship between solar wind and geomagnetic indices and the flux of relativistic electrons at synchronous orbit. Nagai²¹ has shown that the average flux of electrons with energies greater than 2 MeV at synchronous orbit is well estimated by applying a 20-day linear prediction filter relating the daily ΣKp to the electron flux. The following calculation was used to estimate the daily fluence of electrons with energies greater than 300 keV from the flux of electrons with energies greater than 2 MeV obtained from the direct application of Nagai's filter. We assume that the electrons have a spectral shape given by²³

$$dJ/dE = (dJ/dE)_0 \exp(-E/E_0) \text{ (cm}^2\text{/sec-ster-keV)} \quad (1)$$

with $E_0 = 600$ keV. A typical value for $(dJ/dE)_0$ is 1.3×10^4 . The flux above energy E_L is then given by the double integral over solid angle and energy:

$$J = \int_0^{4\pi} \int_{E_L}^{\infty} (dJ/dE)_0 \exp(-E/E_0) d\Omega dE$$

Then

$$J = 4\pi (dJ/dE)_0 E_0 \exp(-E_L/E_0) \quad (3)$$

To compare the flux above two different energy levels, E_1 and E_2 , we can take the ratio $R = J_1/J_2$, which is given by

$$R = \exp [(E_2 - E_1)/E_0] . \quad (4)$$

If E_2 is 2 MeV and E_1 is 300 keV, then the ratio for $E_0 = 600$ keV is about 17. If the instantaneous integral flux > 2 MeV, $J(> 2 \text{ MeV})$, is known, then the average daily fluence > 300 keV is given by

$$F = R(300 \text{ keV}/2 \text{ MeV}) J(> 2 \text{ MeV}) \Delta\Omega \Delta t , \quad (5)$$

where $J(> 2 \text{ MeV})$ is the instantaneous integral flux averaged over a day of electrons with energies greater than 2 MeV. For $\Delta\Omega = 4\pi$ and $\Delta t = 86400$ s, $F = 1.85 \times 10^7 J(> 2 \text{ MeV})$.

This technique was used to estimate the average daily fluence for each day that a discharge occurred on SCATHA. Figure 8 shows the number of days with discharges as a function of the average daily fluence of electrons with energies greater than 300 keV obtained from the linear prediction filter. The filter derived by Nagai peaks two days before the day of the estimate and is in fact negative for zero time lag. This agrees with the temporal behavior of H_{ic} electrons at synchronous orbit.²⁴

We previously developed a neural network to model the temporal behavior of > 3 MeV electrons at geosynchronous orbit based on model inputs consisting of ten consecutive days of the daily sum of the Planetary Magnetic Index, ΣKp .²⁵ The neural network model provides results that are significantly more accurate than those from linear prediction filters. In order to compare the results for the neural network model with those from Nagai's linear prediction filter, we have

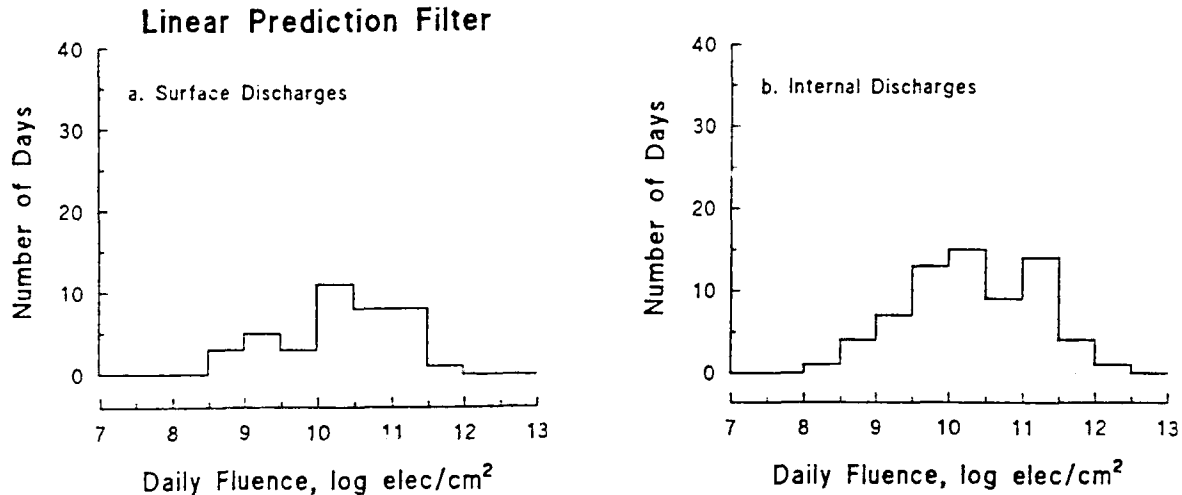


Figure 8. Occurrence of discharges as a function of the daily fluence of electrons with energies greater than 300 keV as estimated by a linear prediction filter model.

scaled the daily fluence obtained from the neural network for 3 MeV to 300 keV. The scaling factor, R , from Eq. (2) is 90. Figure 9 shows the number of days with discharges as a function of the average daily fluence of electrons with energies greater than 300 keV obtained from the neural network model.

From Figures 8 and 9, it is apparent that surface discharges are not well ordered with respect to the daily fluence of ME (scaled from HE) electrons using either technique. Nor are the internal discharges ordered by the daily fluence obtained from the linear prediction filter. However, there is a sharp increase in the number of days with internal discharges when the neural network model estimates the daily fluence of 300 keV electrons to be greater than 10^{10} cm^{-2} (equivalent to the daily fluence of 3 MeV electrons being greater than $1.1 \times 10^8 \text{ cm}^{-2}$). Using a forecasting technique such as that described by Koons and Gorney,²⁵ the neural network model could be used to forecast days when internal discharges might occur on synchronous spacecraft.

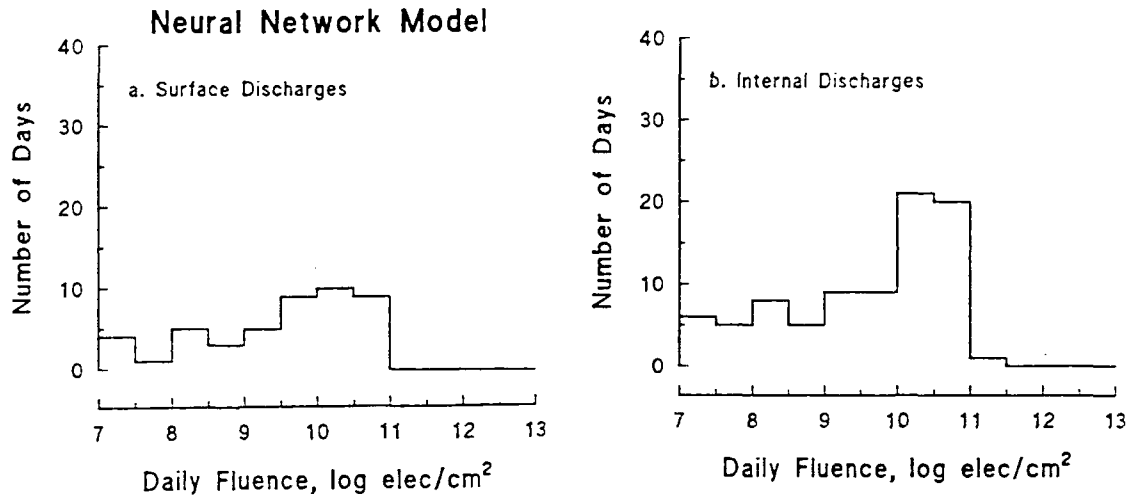


Figure 9. Occurrence of discharges as a function of the daily fluence of electrons with energies greater than 300 keV as estimated by neural network model.

SUMMARY

Pulses detected on SCATHA have been divided into two groups: those from surface discharges, which occurred when the Kapton and quartz fabric test samples on the surface of the vehicle were charged relative to the vehicle frame, and those from internal discharges, which occurred when the test samples on the surface were not charged. The amplitudes of the pulses from the surface discharges tend to be larger than those from the internal charges.

The occurrence of the two types of pulses from the discharges differs in a number of ways. The internal discharges occur much more frequently near the perigee of the SCATHA satellite while the surface discharges occur about evenly over the range of altitudes from 5.5 to 8 R_E . The surface discharges have a strong peak in their occurrence at local midnight, decreasing toward local morning, while the internal discharges have a broader maximum centered on the day side of the Earth. Both types tend to occur while the Earth's magnetic field is disturbed. Although few surface discharges occur when K_p is less than 4, a modest number of internal discharges occur under quiet to normal conditions. Surface discharges have a strong tendency to occur when the flux of 10's of keV electrons is high while internal discharges occur when the flux of 100's of keV electrons is high and the flux of 10's of keV electrons is low.

The statistics of surface discharges on the SCATHA spacecraft are dominated by the single charging event on September 22, 1982. The largest amplitude discharges and the most serious satellite anomalies occurred during this event while the spacecraft was in sunlight near perigee at 0430 local time.

The data from the SCATHA spacecraft have confirmed all aspects of the "spacecraft charging hypotheses" first postulated as a cause of satellite anomalies in the mid 1970's. A direct connection has now been verified between the energetic electron environment, the surface and internal charging of materials on the vehicle, electrostatic discharges, and spacecraft anomalies.

REFERENCES

1. Pike, C. P. and Bunn, M. H., "A Correlation Study Relating Spacecraft Anomalies to Environmental Data," *Spacecraft Charging by Magnetospheric Plasmas*, Progress in Astronautics and Aeronautics, Vol. 47, edited by A. Rosen, AIAA, New York, 1976, pp. 45-60.
2. McPherson, D. A. and Schober, W. R., "Spacecraft Charging at High Altitude: The SCATHA Satellite," *Spacecraft Charging by Magnetospheric Plasmas*, Progress in Astronautics and Aeronautics, Vol. 47, edited by A. Rosen, AIAA, New York, 1976, pp. 15-30.
3. Inouye, G. T., "Spacecraft Charging Anomalies on the DSCS-II, Launch 2 Satellites," *Proceedings of the Spacecraft Charging Technology Conferences*, edited by C. P. Pike and R. R. Lovell, Air Force Geophysics Laboratory, Hanscom, MA, AFGL-TR-77-0051, Feb. 1977, pp. 829-852.
4. DeForest, S. E., "Spacecraft Charging at Synchronous Orbit," *Journal of Geophysical Research*, Vol. 77, Feb. 1972, pp. 651-659.
5. Shaw, R. R., Nanevich, J. E., and Adamo, R. C., "Observations of Electrical Discharges Caused by Differential Satellite Charging," *Spacecraft Charging by Magnetospheric Plasmas*, Progress in Astronautics and Aeronautics, Vol. 47, edited by A. Rosen, AIAA, New York, 1976, pp. 61-76.
6. Garrett, H. B., "The Charging of Spacecraft Surfaces," *Reviews of Geophysics and Space Physics*, Vol. 19, Nov. 1981, pp. 577-616.
7. Vampola, A. L., "Thick Dielectric Charging on High-Altitude Spacecraft," *Journal of Electrostatics*, Vol. 20, Jan. 1987, pp. 21-30.
8. Muelenberg, A. Jr., "Evidence for a New Discharge Mechanism for Dielectrics in a Plasma," *Spacecraft Charging by Magnetospheric Plasmas*, Progress in Astronautics and Aeronautics, Vol. 47, edited by A. Rosen, AIAA, New York, 1976, pp. 237-246.
9. Robinson, P. A. Jr., "Spacecraft Environmental Anomalies Handbook," Geophysics Laboratory, Hanscom, MA, GL-TR-89-0222, Aug. 1989, pp. 3-1 - 3-7.
10. Stevens, J. R. and Vampola, A. L., "Description of the Space Test Program P78-2 Spacecraft and Payloads," The Aerospace Corporation, El Segundo, CA, SAMSO TR-78-24, Oct. 1978.
11. Fennell, J. F., "Description of P78-2 (SCATHA) Satellite and Experiments," *The IMS Source Book*, edited by C. T. Russell and D. J. Southwood, American Geophysical Union, Washington, DC, 1982, pp. 65-81.
12. Koons, H. C., Mizera, P. F., Fennell, J. F., and Hall, D. F., "Spacecraft Charging Results from the SCATHA Satellite," *Astronautics and Aeronautics*, Vol. 18, Nov. 1980, pp. 44-47.

13. Koons, H. C., "Aspect Dependence and Frequency Spectrum of Electrical Discharges on the P78-2 (SCATHA) Satellite," *Proceedings of the Spacecraft Charging Technology Conference III*, NASA Conference Publication 2182, Nov. 1980, pp. 478-492.
14. Koons, H. C., "Summary of Environmentally Induced Electrical Discharges on the P78-2 (SCATHA) Satellite," *Journal of Spacecraft and Rockets*, Vol. 20, Sept.-Oct. 1983, pp. 425-431.
15. Koons, H. C. and Cohen, H. A., "Plasma Waves and Electrical Discharges Stimulated by Beam Operations on a High Altitude Satellite," *Artificial Particle Beams in Space Plasma Studies*, edited by Björn Grandal, Plenum Press, New York, 1982, pp. 111-120.
16. Koons, H. C., Mizera, P. F., Roeder, J. L., and Fennell, J. F., "Severe Spacecraft-Charging Event on SCATHA in September 1982," *Journal of Spacecraft and Rockets*, Vol. 25, May-June 1988, pp. 239-243.
17. Lanzerotti, L. J., Roberts, C. S., and Brown, W. L., "Temporal Variations in the Electron Flux at Synchronous Altitudes," *Journal of Geophysical Research*, Vol. 72, Dec. 1967, pp. 5893-5902.
18. Williams, D. J., and Mead, G. D., "Nightside Magnetospheric Configuration as Obtained from Trapped Electrons at 1100 Kilometers," *Journal of Geophysical Research*, Vol. 70, July 1965, 3017-3029.
19. Pfitzer, K. A., Lezniak, T. W., and Winckler, J. R., "Experimental Verification of Drift-shell Splitting in the Distorted Magnetosphere," *Journal of Geophysical Research*, Vol. 74, Sept. 1969, 4687-4693.
20. Baker, D. N., Blake, J. B., Klebesadel, R. W., and Higbie, P. R., "Highly Relativistic Electrons in the Earth's Outer Magnetosphere, I. Lifetimes and Temporal History 1979-1984," *Journal of Geophysical Research*, Vol. 91, April 1986, pp. 4265-4276.
21. Nagai, Tsugunobu, "Space Weather Forecast: Prediction of Relativistic Electron Intensity at Synchronous Orbit," *Geophysical Research Letters*, Vol. 15, May 1988, pp. 425-428.
22. Baker, D. N., McPherron, R. L., Cayton, T. E., and Klebesadel, R. W., "Linear Prediction Filter Analysis of Relativistic Electron Properties at 6.6 R_E ," *Journal of Geophysical Research*, Vol. 95, Sept. 1990, pp. 15,133-15,140.
23. Baker, D. N., Blake, J. B., Gorney, D. J., Higbie, P. R., Klebesadel, R. W., and King, J. H., "Highly Relativistic Magnetospheric Electrons: A Role in Coupling to the Middle Atmosphere?," *Geophysical Research Letters*, Vol. 14, Oct. 1987, pp. 1027-1030.
24. Paulikas, G. A. and J. B. Blake, "Modulation of Trapped Energetic Electrons at 6.6 R_E by the Direction of the Interplanetary Magnetic Field," *Geophysical Research Letters*, Vol. 3, May 1976, pp. 277-283.

TECHNOLOGY OPERATIONS

The Aerospace Corporation functions as an "architect-engineer" for national security programs, specializing in advanced military space systems. The Corporation's Technology Operations supports the effective and timely development and operation of national security systems through scientific research and the application of advanced technology. Vital to the success of the Corporation is the technical staff's wide-ranging expertise and its ability to stay abreast of new technological developments and program support issues associated with rapidly evolving space systems. Contributing capabilities are provided by these individual Technology Centers:

Electronics Technology Center: Microelectronics, solid-state device physics, VLSI reliability, compound semiconductors, radiation hardening, data storage technologies, infrared detector devices and testing, electro-optics, quantum electronics, solid-state lasers, optical propagation and communications; cw and pulsed chemical laser development, optical resonators, beam control, atmospheric propagation, and laser effects and countermeasures; atomic frequency standards, applied laser spectroscopy, laser chemistry, laser optoelectronics, phase conjugation and coherent imaging, solar cell physics, battery electrochemistry, battery testing and evaluation.

Mechanics and Materials Technology Center: Evaluation and characterization of new materials: metals, alloys, ceramics, polymers and their composites, and new forms of carbon; development and analysis of thin films and deposition techniques; nondestructive evaluation, component failure analysis and reliability; fracture mechanics and stress corrosion; development and evaluation of hardened components; analysis and evaluation of materials at cryogenic and elevated temperatures; launch vehicle and reentry fluid mechanics, heat transfer and flight dynamics; chemical and electric propulsion; spacecraft structural mechanics, spacecraft survivability and vulnerability assessment; contamination, thermal and structural control; high temperature thermomechanics, gas kinetics and radiation; lubrication and surface phenomena.

Space and Environment Technology Center: Magnetospheric, auroral and cosmic ray physics, wave-particle interactions, magnetospheric plasma waves; atmospheric and ionospheric physics, density and composition of the upper atmosphere, remote sensing using atmospheric radiation; solar physics, infrared astronomy, infrared signature analysis; effects of solar activity, magnetic storms and nuclear explosions on the earth's atmosphere, ionosphere and magnetosphere; effects of electromagnetic and particulate radiations on space systems; space instrumentation; propellant chemistry, chemical dynamics, environmental chemistry, trace detection; atmospheric chemical reactions, atmospheric optics, light scattering, state-specific chemical reactions and radiative signatures of missile plumes, and sensor out-of-field-of-view rejection.